N87-16418

DEVELOPMENT OF HIGH-EFFICIENCY SOLAR CELLS ON SILICON WEB

WESTINGHOUSE RESEARCH AND DEVELOPMENT CENTER

D. L. Meier

Topics

- Determination of defect in web silicon which limits minority carrier diffusion length
- Passivation of defects by low energy, high dose hydrogen ion implantation
- Fabrication of web and float zone cells

Location of TEM, LBIC, and DLTS Samples in Web Cell

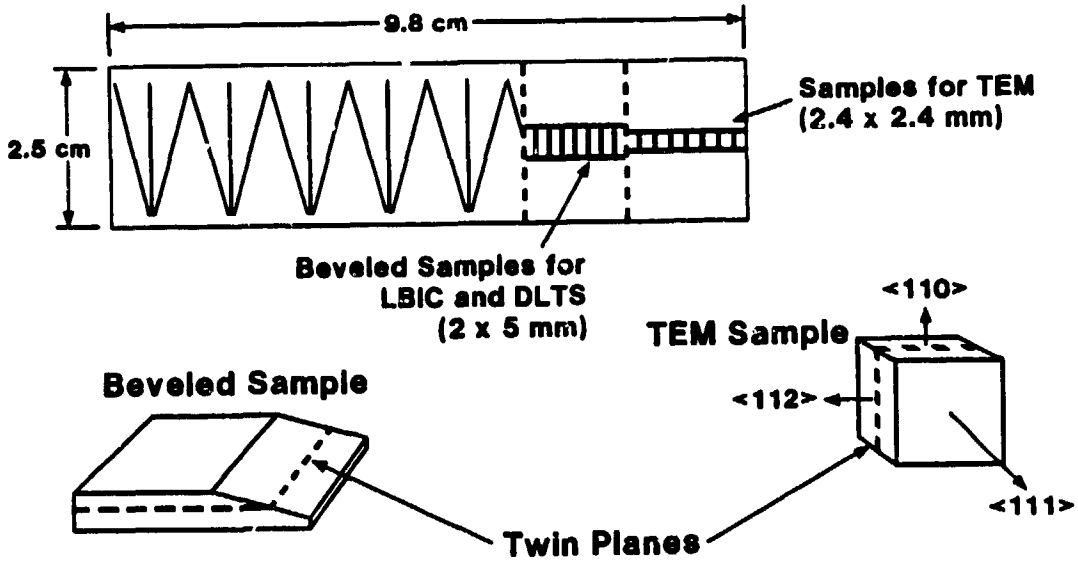

Cross-Sectional TEM Sample Preparation

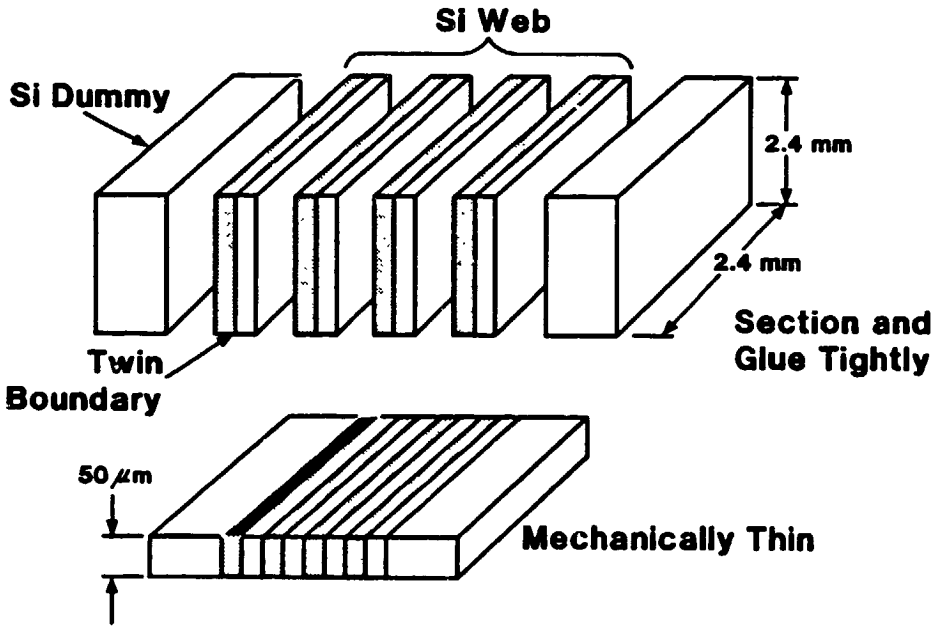

Cross-Sectional TEM Sample

FORMATION OF THIN FOIL AT EDGE OF HOLE

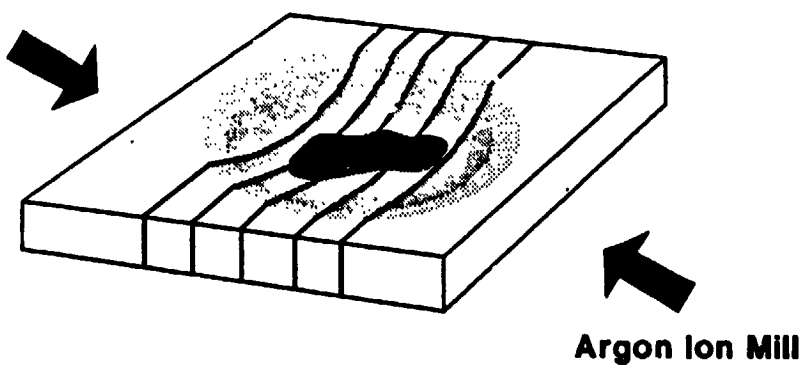

Electrical Parameters of Cells Examined by Cross-Sectional TEM

Cell	L_n (SPV) (μm)	J_{sc} (mA/cm^2)	V_{oc} (V)	FF	η (%)
17C	12	23.4	0.514	0.79	9.5
38A	156	31.0	0.584	0.79	14.9
40C	19	24.3	0.525	0.78	10.0
69A	135	31.2	0.580	0.78	14.3

Notes:

1. Cells have p-base (boron-doped) of nominal 4 ohm-cm resistivity.
2. Cell size is (2.0 x 9.8) cm or (2.5 x 9.8) cm.
3. Cells tested at 100 mW/cm^2. AM1 spectrum at room temperature.

Cell 40C: Low-Efficiency Twin Plane Region

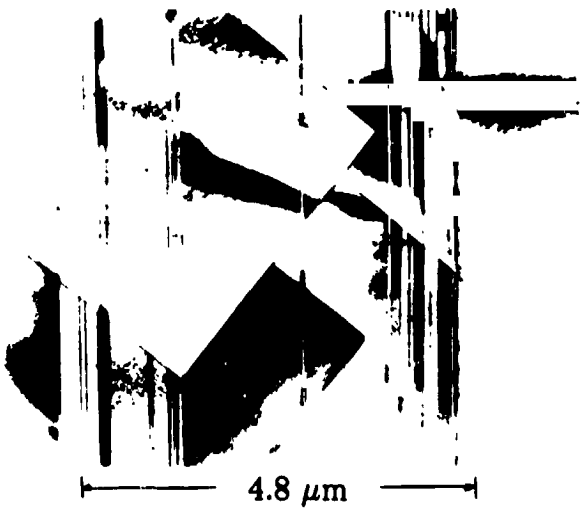

Twin Plane Vertical

Twin Plane Region:
Numerous Alternating Twins

Cell 40C: Low Efficiency

—4.8 μm—

Twin Plane Tilted; Twins Out of Contrast

Numerous Dislocations Adjacent
to Twin Boundaries

TEM micrograph showing dislocations in the bulk of low-efficiency cell 40C (10.0%). Note large density of dislocations in the heavily twinned region near the top of the micrograph.

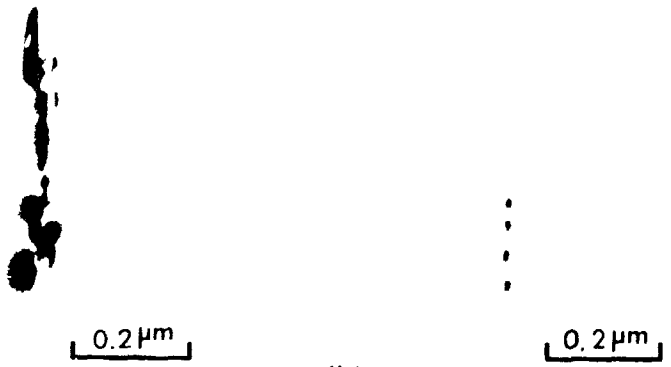

TEM micrograph showing possibility of impurity decoration at dislocations in low-efficiency cell 40C (10.0%): (a) two-beam dynamical condition showing strain fields, and (b) weak quasi-kinematical condition with strain fields minimized.

Cell 69A: High Efficiency

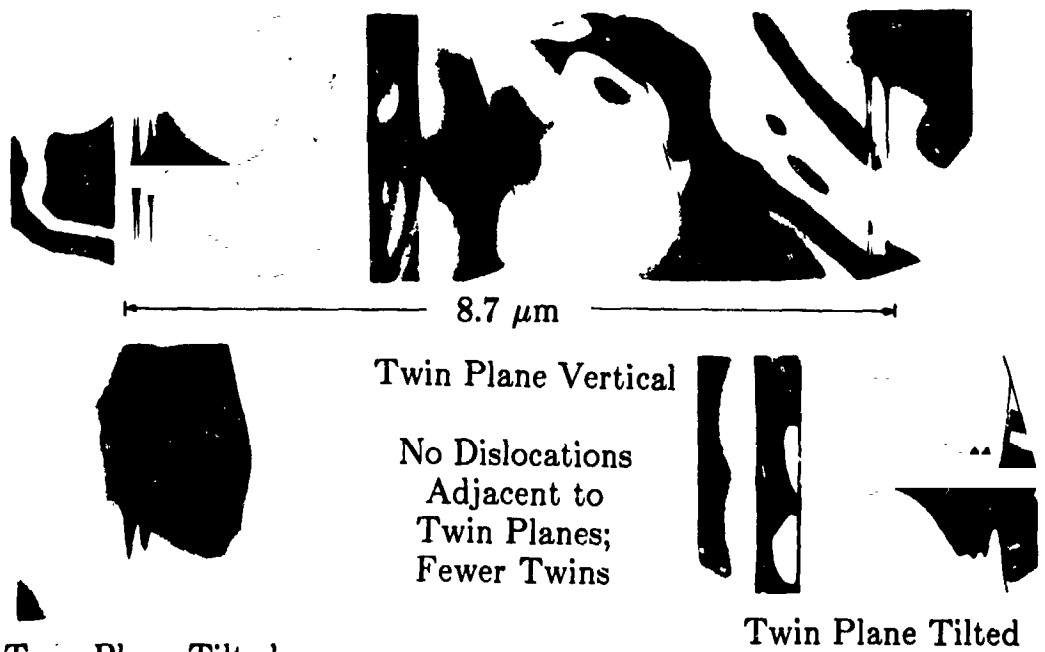

Summary of TEM Observations with Electrical Parameters

Cell	L_n (SPV) (μm)	η (%)	Number of Twin Boundaries	Width of Heavily Twinned Region (μm)	Dislocation Density (cm^{-2})	
					Twinned Region	Bulk
17C	12	9.5	27	5.7	2×10^8	$\simeq 10^6$
38A	156	14.9	5	3.6	None Observed	One Observed
40C	19	10.0	41	4.8	3×10^8	$\simeq 10^6$
69A	135	14.3	13	8.7	None Observed	None Observed

Note: Detection limit for dislocation density by TEM is 10^4 - 10^5 cm^{-2}.

Sensing the Electrical Activity of the Twin Plane with Laser-Induced Current

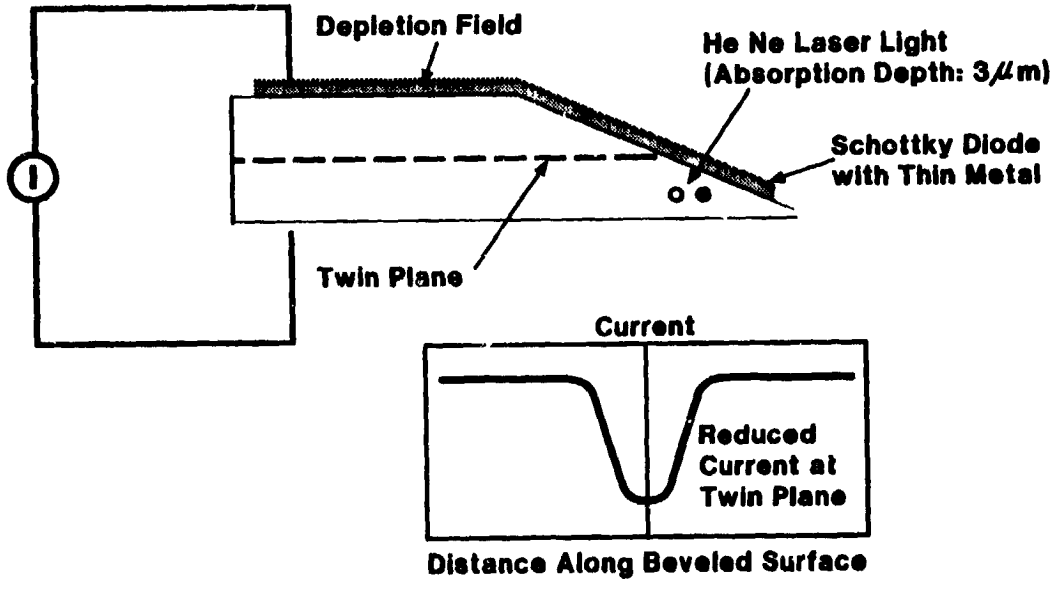

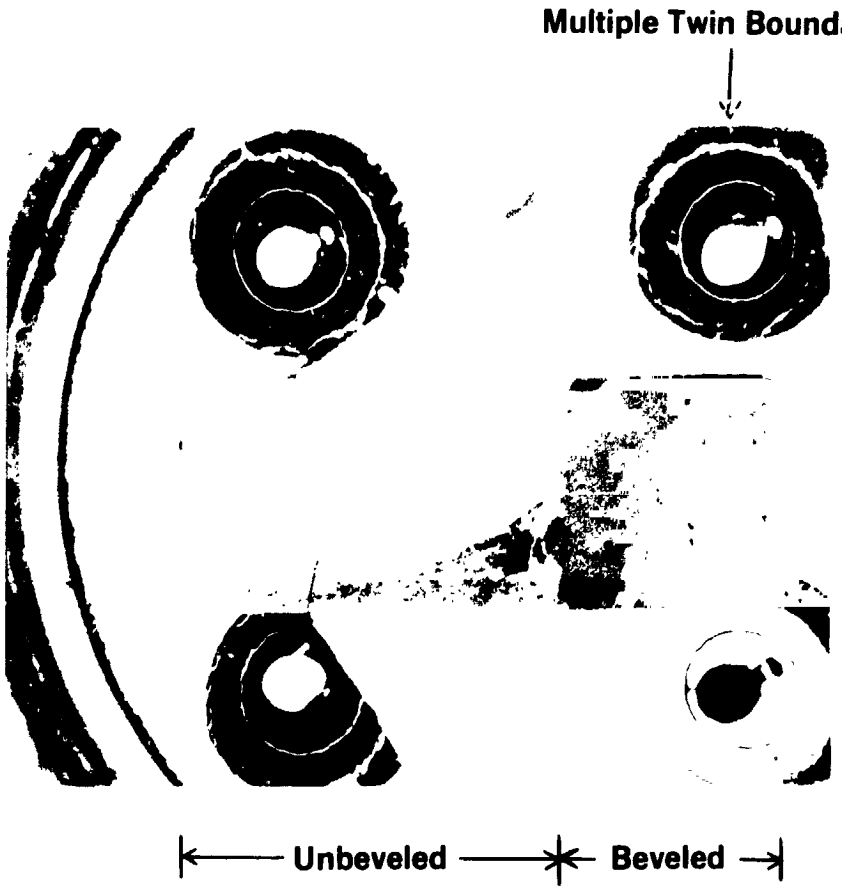

Photograph of a (2 × 5) mm beveled sample prepared from cell 17C (9.5%) and mounted on a TO-5 header. Shown are the area of the sample covered with semitransparent metal to form the Schottky diode and the lines formed where the twin boundaries emerge from the beveled surface. (Sample #1, Run TP-10)

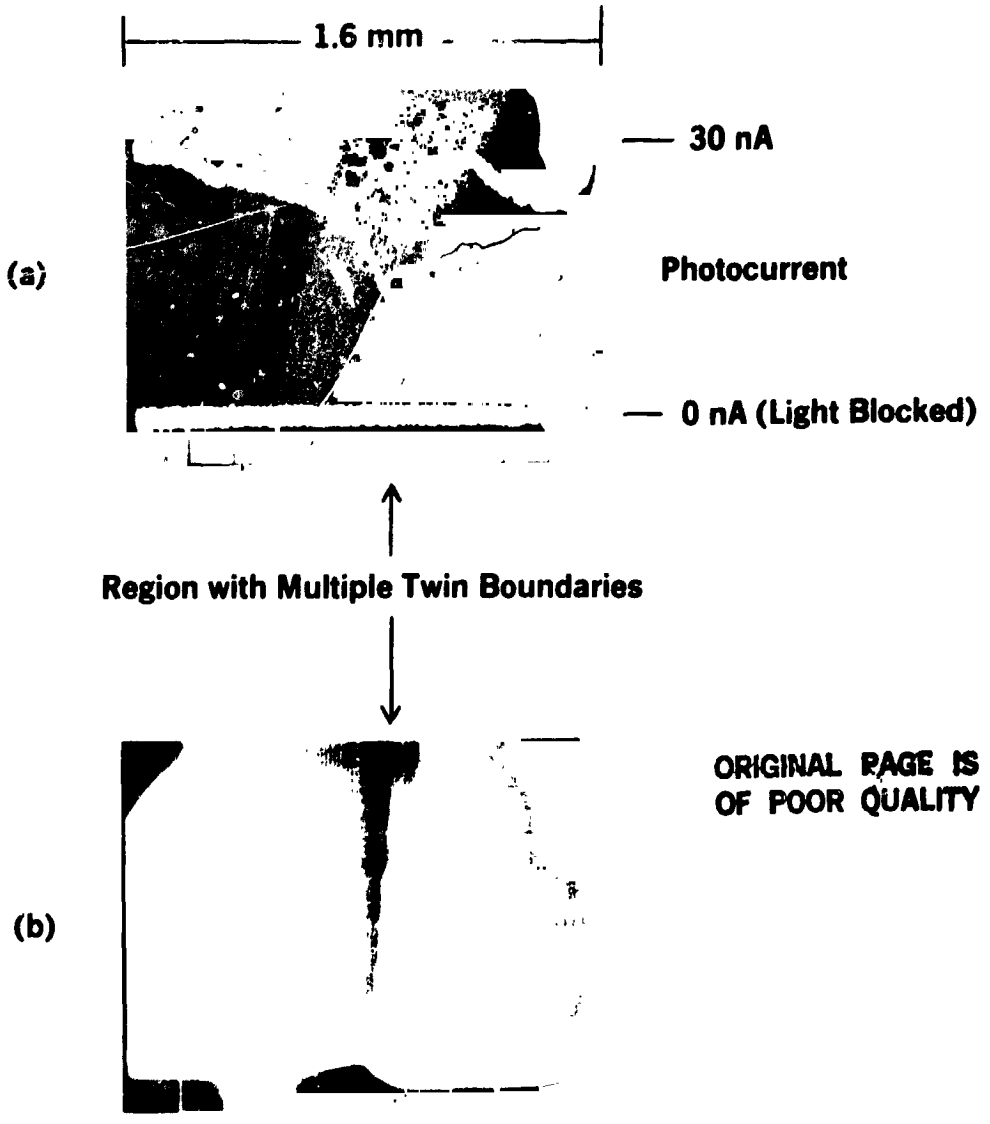

LBIC scans of beveled sample prepared from cell 17C (9.5%): (a) line scan showing 50% decrease in photocurrent in the vicinity of the twinned region as the laser beam is scanned down the beveled surface across the twin boundaries; (b) area scan showing uniform dark bands associated with excessive recombination within and near the twinned region. (Sample #1, Run TP-10)

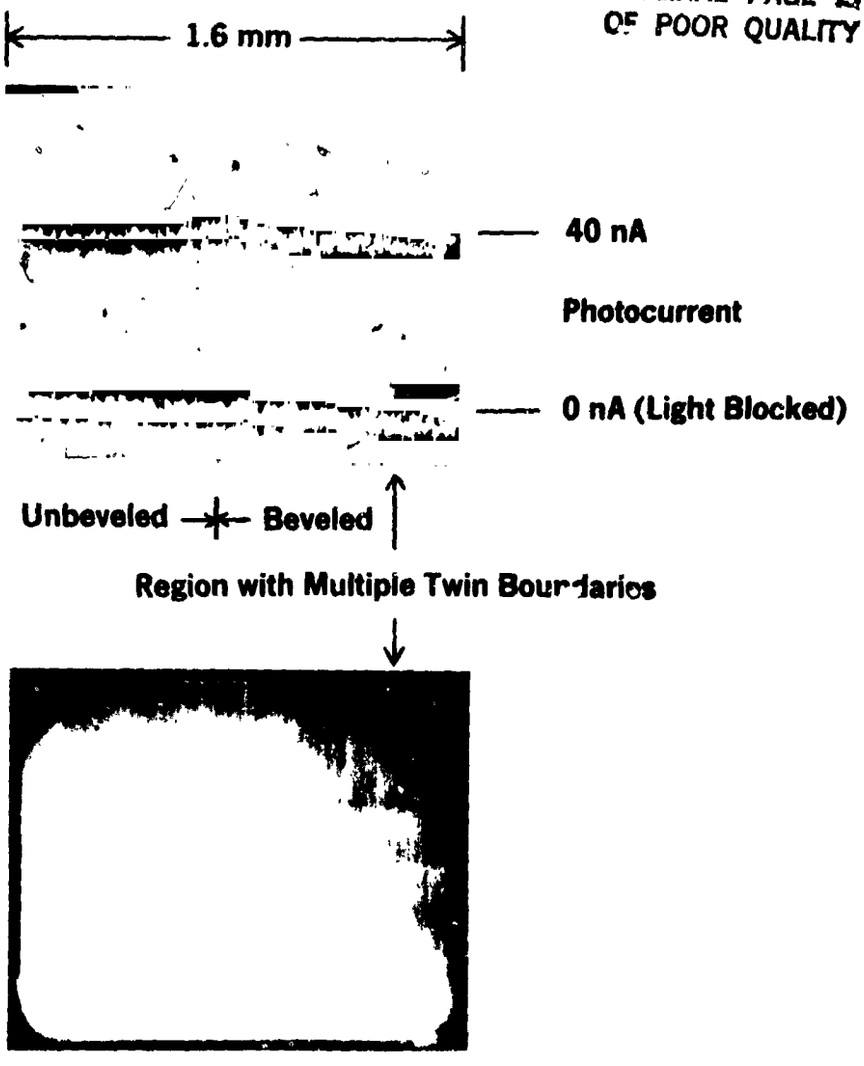

LBIC scans of beveled sample prepared from cell 38A (14.9%): (a) line scan showing no decrease in photocurrent in the vicinity of the twinned region; (b) area scan showing no features associated with the twinned region. (Sample #10, Run TP-10)

Comparison of Minority Carrier Diffusion Length with Twin Plane Depth

Cell	η (%)	L_n (SPV) (μm)	Twin Plane Depth (μm)	Cell Thickness (μm)
17C	9.5	12	60	158
38A	14.9	156	55	110
40C	10.0	19	65	148
69A	14.3	135	70	155

Impurity Depth Profile by DLTS

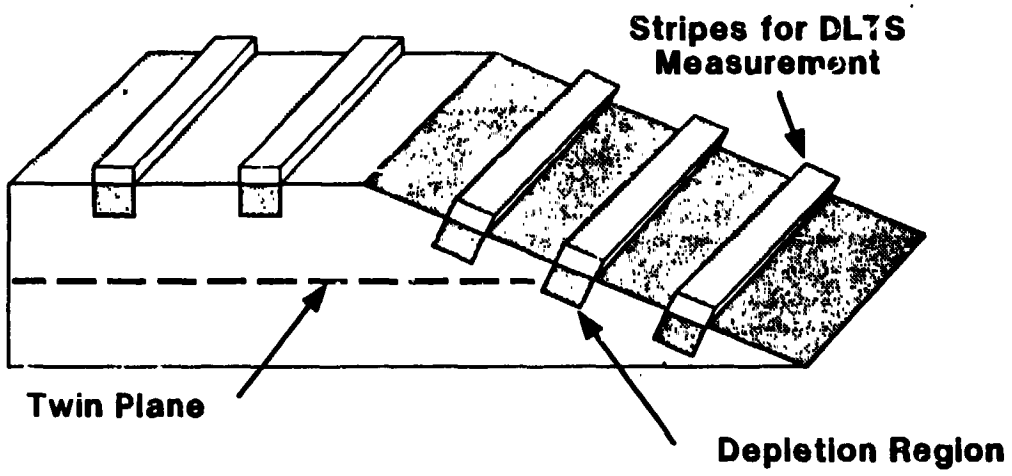

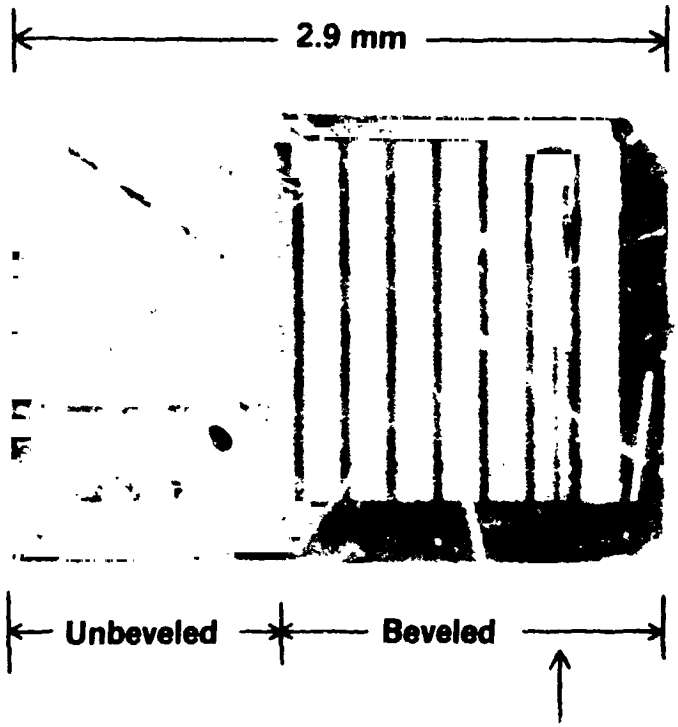

Photograph of a beveled sample prepared from cell 17C (9.5%) showing Schottky diodes in the form of stripes for DLTS measurements. Note that the second stripe from the right is located directly over the lines which indicate twin boundaries emerging from the beveled surface. (Sample #3, Run TP-10)

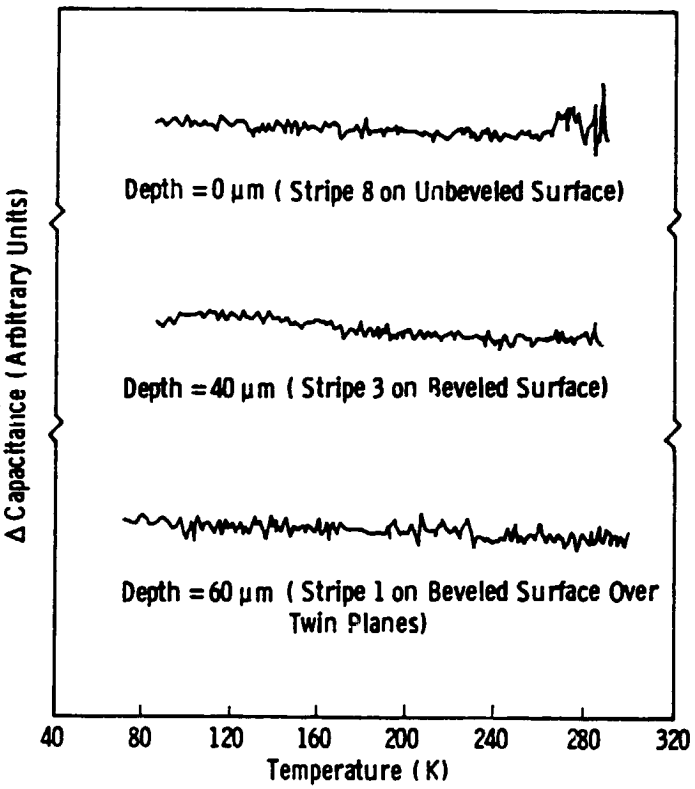

DLTS scans for stripes on a beveled sample prepared from cell 17C (9.5%) showing that the concentration of electrically-active point defects is below the DLTS detection limit of 3×10^{11} cm^{-3}. (Sample #5, Run TP-10)

Conclusions

1. **Low Efficiency (9.5%) Web Cells Have Many Boundaries (≥27) and a High Dislocation Density**
   - **2×10^{8} cm^{-2} in Heavily Twinned Region**
   - **$\approx 10^{6}$ cm^{-2} in Bulk**
2. **High Efficiency (14.9%) Web Cells Have Fewer Twin Boundaries (≤13) and Low Dislocation Density ($<10^{4}$-$10^{5}$$cm^{-2}$)**
3. **A Significant Fraction of the Dislocations are Decorated with Precipitates**
4. **Twin Boundaries Without Dislocations are Transparent to Minority Carriers But Those with Dislocations are Electrically Active**
5. **In Low Efficiency Cells the Diffusion Length is Controlled by Dislocations Alone or Dislocations with Precipitates, Not by Dissolved Impurities**

Effect of Hydrogen Ion Implantation on Web Cells

Web Cell ID	H^+ Implant	J_{sc} (mA/cm^2)	V_{oc} (V)	FF	η (%)	SPV L_n (μm)
48-1	No	32.0	0.510	0.729	11.9	19
48H-1	Yes	36.4	0.574	0.770	16.1	120
52-1	No	36.8	0.586	0.773	16.7	130
52H-1	Yes	36.7	0.589	0.757	16.4	> 200

Notes:

1. Implant Conditions: 1500 eV, 2 mA/cm^2, 2 minutes with no stage cooling.
2. Hydrogen was implanted into the emitter side of the cells after boron and phosphorus diffusions.
3. Cell Size: 1 x 1 cm.
4. Test Conditions: AM1 (tungsten/halogen lamp), 100 mW/cm^2, room temperature (Run Cell-4).
5. Starting web material was boron-doped to 4 ohm-cm.
6. Anti-reflective coating: 600 Å ZnS and 1000 Å MgF_2

Process Sequence for Metal Contact to Silicon Along Grid Line Openings in Oxide

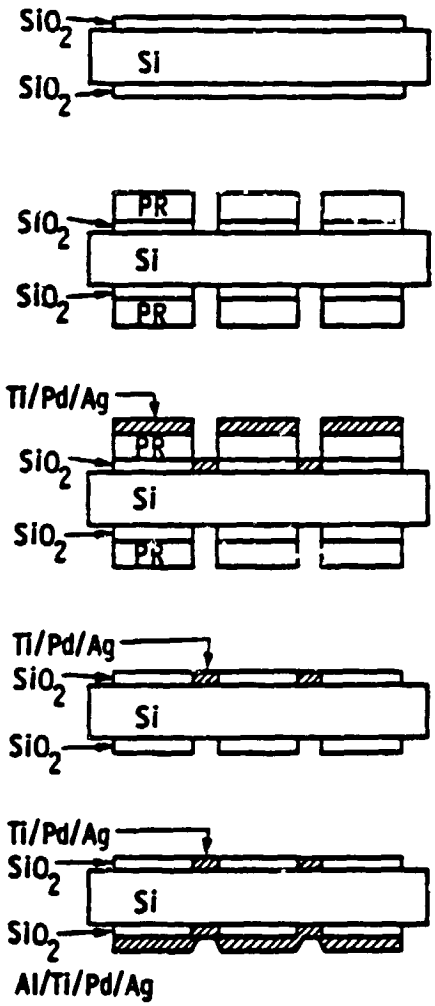

1. Oxide-Passivation Layers on Diffused Silicon
2. Grid Line Contact Windows Etched in Oxide Front and Back.
3. Front Metal Evaporation (Ti/Pd/Ag)
4. Metal Rejection; Front Grid Lines Contact Silicon
5. Back Metal Evaporation (Al/Ti/Pd/Ag) ; Back Grid Lines Contact Silicon

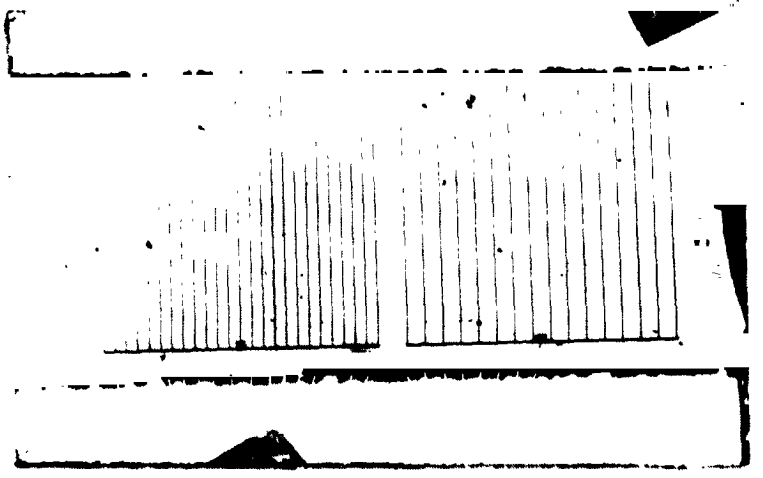

Cells Produced by the High-Efficiency Process (Run Cell-3)

Cell ID	Substrate	J_{sc} (mA/cm^2)	V_{oc} (V)	FF	η (%)	QE L_n (μm)	τ_{ocd} (μs)	Thickness (μm)
A-2	web	37.1	0.571	0.765	16.2	149	31	124
C-2	web	36.0	0.584	0.769	16.2	62	22	127
E-2	web	37.5	0.576	0.762	16.5	116	79	140
3FZH-7	float zone	35.9	0.626	0.812	18.3	210	36	394

Notes:

1. Cell Size: 2 x 2 cm
2. Test Conditions: AM1 (tungsten/halogen lamp). 100 mW/cm^2 room temperature.
3. Web substrates were boron-doped to 4 ohm-cm (nominal); float zone substrates were boron-doped to 0.2 ohm-cm (Wacker 100)
4. Surface Passivation: 100 Å SiO_2 (front and back).
5. Anti-reflective coating: 430 Å ZnS and 1000 Å MgF_2 (evaporated)
6. Back surface reflector: 1000 Å Aluminum.
7. Forward current for τ_{ocd} measurement: 150 mA (~ I_{sc})

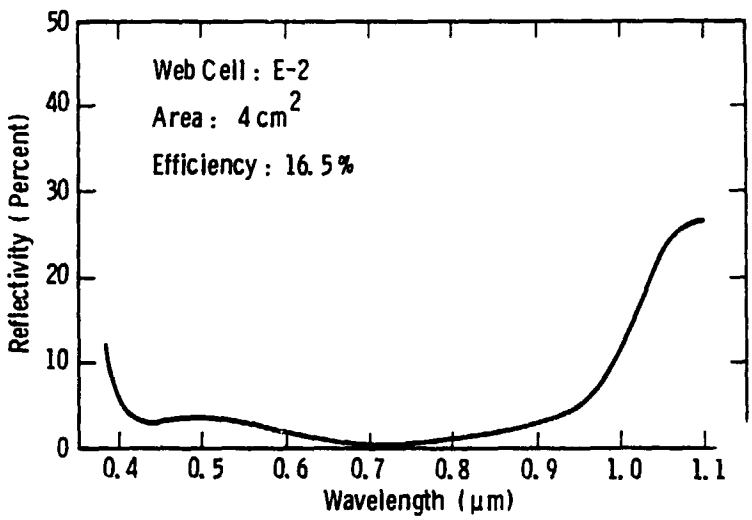

Reflectivity versus wavelength for Web Cell E-2 from Run Cell-3. Cell has double layer anti-reflective coating (430 Å ZnS and 1000 Å MgF_2) evaporated onto a passivated (100 Å SiO_2) silicon surface

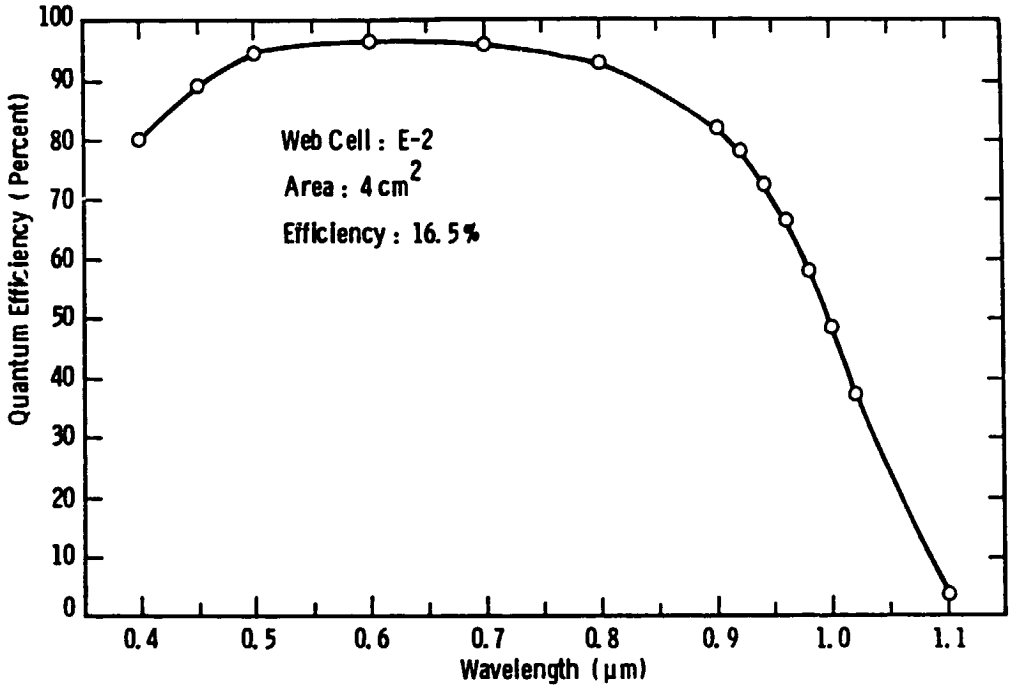

Quantum efficiency versus wavelength for web cell E-2 from Run Cell-3. Cell has surface passivation (100 Å SiO_2), double layer anti-reflective coating (430 Å ZnS and 1000 Å MgF_2) and aluminum back surface reflector. Web substrate is boron-doped to 4 ohm-cm and efficiency is 16.5%. Note high short wavelength response

Future Work for Web Cells

- **Decrease resistivity from 4 ohm-cm to 0.2 ohm-cm**
- **Incorporate H^+ implantation to improve diffusion length to 100 microns or more**
- **Retain oxide passivation, double layer AR coating, aluminum back surface reflector and standard cell thickness (120 microns)**
- **Anticipate efficiency > 17%**

Summary

- Primary defect in silicon web cells which limits diffusion length is a dislocation decorated with impurity precipitates
- Precipitate may be SiO_x
- Twin boundaries in web cells are electrically benign
- Diffusion length and cell efficiency can be improved significantly in web cells by H^+ implantation at 1500 eV, 2 mA/cm^2 for 2 minutes
- Cells (4 cm^2) have been fabricated from web substrates boron-doped to 4 ohm-cm having:

$$\eta = 16.5\%$$

$$\tau_{ocd} = 79\ \mu s$$

PROCESSING

Brian D. Gallagher, Chairman

E. Kolawa, of the California Institute of Technology (Caltech), discussed the investigation of amorphous W-Zr and W-N alloys as diffusion barriers in silicon metallization schemes. Data were presented showing that amorphous W-Zr crystallizes at 900°C, which is 200°C higher than amorphous W-Ni films, and that both films react with metallic overlayers at temperatures far below the crystallization temperature. Also, W-N alloys (crystalline temperature of 600°C) have been successfully incorporated as a diffusion barrier in contact structures with both Al and Ag overlayers. The thermal stability of the electrical characteristics of shallow n^+p junctions is significantly improved by incorporating W-N layers in the contact system. One important fact demonstrated during this investigation was the critical influence of the deposition parameters during formation of these barriers.

J. Parker, of Electrink, described the processing techniques and problems encountered in formulating metallo-organic decomposition (MOD) films used in contacting structures for thin solar cells. The use of thermogravimetric analysis (TGA) and differential scanning calorimetry (DSC) techniques performed at JPL in understanding the decomposition reactions lead to improvements in process procedures. The characteristics of the available MOD films were described in detail.

R. Vest described the status of the ink-jet printing program at Purdue University. The drop-on-demand printing system has been modified to use MOD inks. Also, an IBM AT computer has been integrated into the ink-jet printer system to provide operational functions and contact pattern configuration. The integration of the ink-jet printing system, problems encountered, and solutions derived were described in detail. The status of ink-jet printing using a MOD ink was discussed. The ink contained silver neodecanoate and bismuth 2-ethylhexanoate dissolved in toluene; the MOD ink decomposition products being 99 wt % Ag, and 1 wt % Bi.

D. Meier, of Westinghouse Electric, described the status of the investigation of laser-assisted solar cell metallization processing. This process was the laser pyrolysis of spun-on metallo-organic silver films by an argon ion laser beam. The MOD film is spun-on an evaporated Ti/Pd film to produce good adhesion. In a maskless process, the argon ion laser "writes" the contact pattern. The film is then built up to obtain the required conductivity using conventional silver plating processes. The Ti/Pd film in the field is chemically etched using the plated silver film as a mask. The width of the contact pattern is determined by the power of the laser. Widths as thin as 20 μm were obtained using 0.66 W of laser power.

Cells fabricated with 50 μm line widths of 4 ohm-cm FZ silicon-produced efficiencies of 16.6% (no passivation) which were equivalent to the best cells using conventional metallization/lithography and no passivation. Funding problems caused the premature cessation of this study before a process could be developed that would eliminate the need for the evaporative Ti/Pd film base.

PROCESSING

R. B. Campbell, of Westinghouse Advanced System Division, described the investigation of simultaneous diffusion of liquid precursors containing phosphorous and boron into dendritic web silicon to form solar cell structures. A novel, simultaneous junction formation technique was developed. The web material was subjected to a high-temperature, short-time pulse from tungsten-halogen flash lamps. Times of 5 to 15 s and temperatures of 1000 to 1150°C were investigated. It was determined that to produce high quality cells, an annealing cycle (nominal 800°C for 30 min) should follow the diffusion process to anneal quenched-in defects. Two ohm-cm n-base cells were fabricated with efficiencies greater than 15%. A cost analysis indicated that the simultaneous diffusion process costs can be as low as 65% of the costs of the sequential diffusion process.

G. A. Rozgonyi, of the Materials Engineering Department of North Carolina State University, discussed their investigation in rapid thermal processing (RTP) of Cz silicon substrates and the attendant effects on defects, denuded zones, and minority carrier lifetime. Preferential chemical etching and x-ray topography was used to delineate defects which were subsequently correlated with minority carrier lifetime; determined by a pulsed MOD test device. The x-ray delineation of grown-in defects was enhanced by a lithium decoration procedure.

Results, thus far, show excellent correlation between process-induced defects. Wafers with optimum RTP and implant processes suitable for solar cell evaluation will be available this summer.

S. J. Fonash, of Pennsylvania State University, investigated the use of low-energy hydrogen implants in the fabrication of high-efficiency crystalline silicon solar cells. The work established that low-energy hydrogen implants result in hydrogen-caused effects in all three regions of a solar cell: emitter, space charge region, and base. In web, Cz, and FZ material, low-energy hydrogen implants reduced surface recombination velocity. In all three, the implants passivated the space charge region recombination centers. In web cells, the implants passivated the base region. This was not the case, however, in the base region of Cz or FZ cells. In the case of web, it is proposed that the hydrogen is able to diffuse into the base region where it can passivate structural damage present in the web in the base. During the course of the investigation, it was established that hydrogen implants can alter the diffusion properties of ion-implanted boron in silicon, but not ion-implanted arsenic.

B. D. Gallagher, of JPL, discussed investigations involving the low-pressure chemical vapor deposition (LPCVD) of polycrystalline silicon. The physical system was described, as was the controlling process parameters and requirements for producing films for use as an integral portion of the solar cell contact system.

The film depositions were done in a conventional hot wall LPCVD reactor equipped with an Alcatel double-stage rotary pump. Both undoped and PH_3-doped polysilicon deposition processes were developed and characterized. Excellent cell structures were obtained using a $[PH_3]/[SiH_4]$ concentration ratio of 250 to 1. The best results were obtained using a film thickness of 1 KÅ, resulting in cell characteristics of: V_{oc} 650.6, I_{sc} 130.0, FF 0.811, and an efficiency of 17.2%. The fill factor of 0.811 attests to the fact that a good ohmic contact was obtained.